11th World Congress on Computational Mechanics (WCCM XI)
5th European Conference on Computational Mechanics (ECCM V)
6th European Conference on Computational Fluid Dynamics (ECFD VI)
E. Oñate, J. Oliver and A. Huerta (Eds)

SIMULATION OF SHAPED-CHARGE JET PENETRATION INTO DRAINED AND UNDRAINED SANDSTONE USING THE MATERIAL POINT METHOD WITH NEW APPROACHES FOR CONSTITUTIVE MODELING

Michael A. Homel*, Rebecca M. Brannon† and James E. Guilkey†

* University of Utah, Mechanical Engineering,
50 S. Central Campus Dr. MEB 2110 Salt Lake City, Utah 84112
e-mail: michael.homel@utah.edu, web page: http://www.homel.org/

†University of Utah, Mechanical Engineering,
50 S. Central Campus Dr. MEB 2110, Salt Lake City, Utah 84112
e-mail: Rebecca.Brannon@utah.edu, web page: http://csmbrannon.net/

† Schlumberger Technology Corporation
1935 South Fremont Drive, Salt Lake City, UT 84104,
e-mail: jguilkey@slb.com

Key words: Material Point Method, Wellbore Perforation, Constitutive Modeling, Geomaterials, Large Deformation, Plasticity

Abstract. Simulation of wellbore completion by shaped-charged jet penetration in porous rock is highly nontrivial and requires a computational method that can support high-rate large deformation, with multiple materials and evolving contact surfaces. A computational approach is presented, using the Uintah open-source computational framework [4] implementation of the material point method along with recent kinematic advancements. A novel constitutive model is used to predict the response of the target material allowing for a dynamically evolving pore fluid pressure within an effective stress framework. Results are presented showing key experimental validation of the trends in penetration depth vs. pore pressure and confining stress, as well as the effect of nonassociativity, statistical variability, and choice of MPM integrator. New visualization methods are presented that provide insight into the material stress state around the penetration channel.

1 INTRODUCTION

Shaped-charge jet perforation is used to improve the fluid flow into a cased wellbore from the surrounding porous rock formation. A set of computational tools has been

developed to model wellbore perforation, so that more efficient designs can be obtained with less experimental cost.

This application presents unique challenges in computational modeling, requiring a method to solve the equations of motion that allows massive deformation, while maintaining the support for path-dependent constitutive models, which are necessary to describe the complex mechanics of porous rock. This precludes both traditional Lagrangian finite elements methods, which would fail due to mesh entanglement, and Eulerian methods, for which advection errors would pollute the state variable history.

The constitutive model of the target material must account for nonlinear elasticity, pressure-dependent strength, porosity effects, and pore fluid effects, all of which may evolve with plastic deformation. For example, depth of penetration typically increases with the ratio of densities of the jet to target material, but the presence of a pore fluid increases the penetration depth despite the increased target density. This behavior can be modeled by the effective-stress principle, but a proper treatment of the effect that allows for an evolving pore pressure requires special numerical solution methods.

2 METHODS

2.1 Solution of the momentum equation

The material point method (MPM) is an arbitrary Lagrangian-Eulerian method that is well suited for wellbore penetration simulations since it allows severe material distortion, while also supporting history-dependent material models. The MPM is implemented in the Uintah open-source computational framework [4] that supports massively parallel simulations.

The original MPM formulation used a point mass (Dirac delta) approximation to compute the integral expressions for the average of the shape function and its gradient across the particle domain, but this led to undesirable behavior when particles crossed cell boundaries. More modern implementations use variants of the generalized interpolation material point method (GIMP) [1], which define an initial finite particle domain that is used to approximate the integral expressions. This approach mitigates the cell-crossing error, but can lead to poor performance and mesh dependence in problems with large rotations or shear deformation, in particular if the particle domain is fixed or has restricted modes of deformation (*e.g.,* square domains deforming to rectangles in 2D) [3].

A further enhancement is the convective particle domain interpolation (CPDI) method, which allows the initial particle domain to deform with the material deformation gradient (*e.g.,* squares deform into parallelograms in 2D), and constructs adaptive alternative grid-based shape functions across the deformed domain to efficiently compute the nodal forces and consistent mass integrals [3]. CPDI improves accuracy and rates of convergence, and also eliminates the extension instability, which causes spurious material separation when particles become stretched over multiple grid cells.

Eliminating the extension instability complicates the implementation of CPDI in par-

allelized codes, since single particles can stretch beyond the boundary cells of a single computational patch. To remedy this, and also allow for controlled numerical fracture (assuming that it is preceded by physical fracture), a new approach was developed for scaling the CPDI integration domain. Figure 1 illustrates the approach for a 2D implementation. Each corner of the initial parallelogram domain that lies outside an allowable radius is scaled to lie on that radius, and a new parallelogram is constructed from the scaled values.

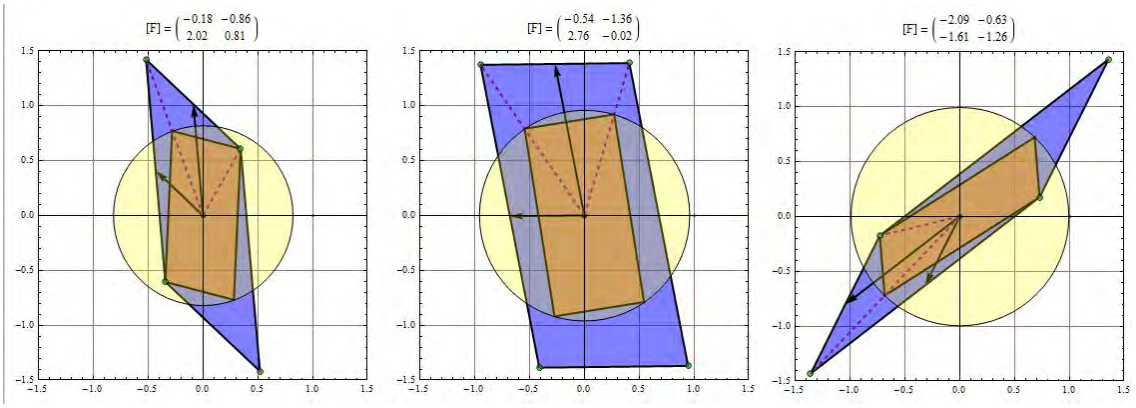

Figure 1: Illustration of the CPDI domain scaling algorithm in 2D

The strategy is similar in 3D, but a pseudo-inverse is used to reconstruct the scaled parallelepiped domain. Only the integration domain is scaled, which does not directly affect the deformation gradient of the particle used to compute the updated stress.

2.2 Jet Description

The shaped-charge penetrator jet is formed from a conical metallic liner compressed by a high-explosive charge. The formation of the jet can be modeled in an MPM simulation as shown in Fig. 2. For wellbore perforation, the standoff distance must be much less than would be ideal for maximum penetration depth, and the velocity profile of the jet continues to evolve (i.e. the jet expands as it translates) as it enters the domain of the target.

For many of the results presented herein, the problem geometry was simplified to an axisymmetric model, which significantly reduces the computational cost. To facilitate validation of the target response, these simulations used an imported jet, defined to match the momentum and kinetic energy flux of an actual shaped charge, where the latter was estimated from flash x-ray and time-of-arrival data. Two approaches were used for the imported jet.

The first approach defines a discrete jet comprising cylinders of uniform density, where the radius, initial spacing and velocity of each cylinder are variables in the jet description [2]. This approach yields a good fit to the momentum flux of the actual jet, but results in

an intermittent impact at the tip of the penetration channel, which may be nonphysical. In some rare cases the discrete jet produced anomalous behavior in the target material, which is thought to result from numerical error associated with the extreme values of the velocity gradient at the boundaries of the jet cylinders. This "*kinematic anomaly*" manifests as extreme deformation of a single particle which can produce localized artifacts in the penetration channel, especially at late times after the penetrator has passed.

The second approach defines a continuous jet description with an initial void fraction defined as a state variable for each particle within the constitutive model. This *expansion strain* is collapsed as the jet hits the target, but unlike the pore collapse in the target material this mode of deformation requires no plastic work. This approach requires special treatment within the plasticity solution algorithm, but has produced promising results. The kinematic anomaly described above has not been observed when using a continuous description of the penetrator.

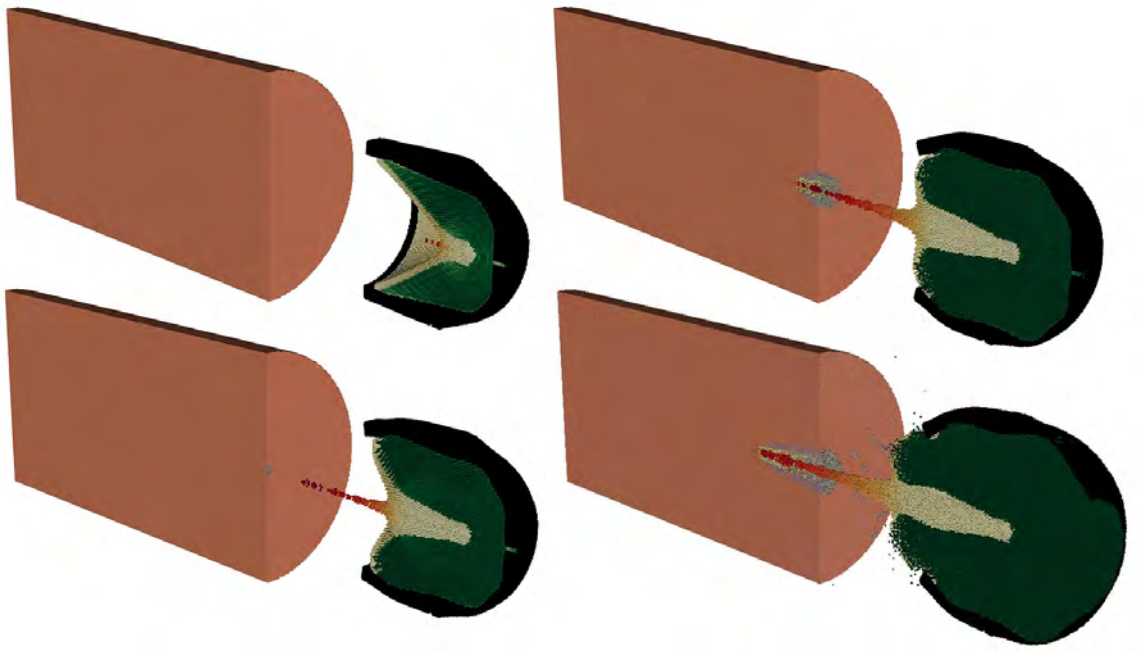

Figure 2: 3D MPM simulation of shaped-charge jet formation and penetration into a sandstone target.

2.3 Target Description

A new phenomenological constitutive model, Arenisca, was developed for the Uintah framework to describe the response of the target material.

Arenicsa uses a two-surface isotropic yield criterion comprising a nonlinear Drucker-Prager shear limit surface and a cap function to allow for pore collapse and to govern the interaction between porosity and shear strength. The cap function evolves via an

empirical crush curve function, describing the dependence of hydrostatic compressive strength on volumetric plastic strain [9]. Other empirical functions [9] describe the elastic response, and allow for nonlinear elasticity with elastic-plastic coupling. Figure 3 shows the hydrostatic load-unload response of the model, which has been fit to experimental data for sandstone, along with a rendering of the initial yield surface in principal stress space.

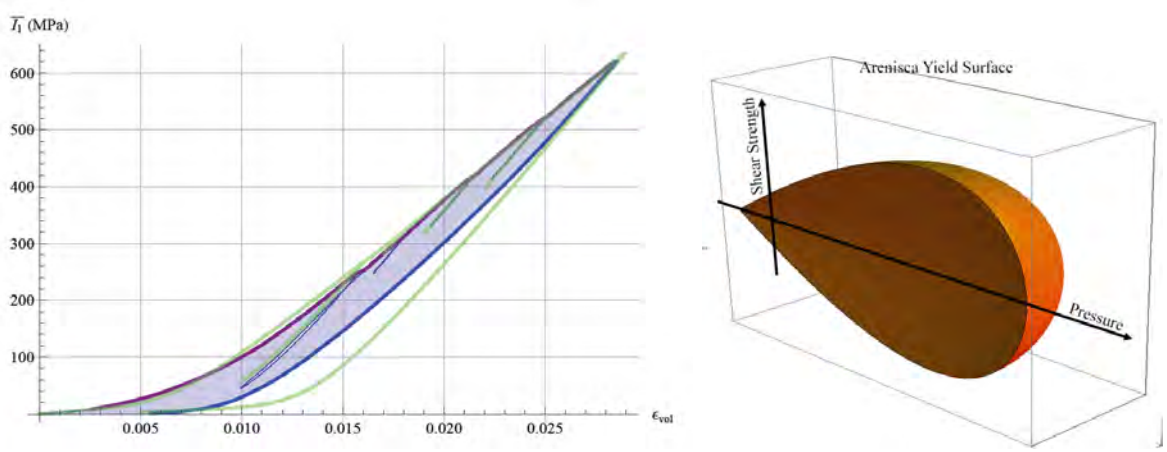

Figure 3: LEFT: Hydrostatic load-unload data for sandstone (green) and the response of the parameterized geomodel (red/blue). The experimental fit neglected the final unload region (thick blue), since there was evidence of creep in the data set. RIGHT: Arenisca yield surface showing a Drucker-Prager shear limit surface with an elliptical cap.

The code supports necessary statistical variability and scale effects in the definition of the strength properties for each particle [7]. The plasticity solution allows for nonassociativity, as an empirical tool to control dilatation. A Duvaut-Lions rate-dependence model captures the apparent increase in strength with loading rate.

A novel approach was taken to model the effect of the pore space fluid. The widely used geomechanics effective stress concept [11] predicts that pore pressure will decrease the shear strength, since the yield criteria are evaluated with the difference between the applied pressure and pore fluid pressure. This effect leads to an increased depth of penetration for an undrained target material, in spite of the increased mass density.

If the porosity is not connected, or the loading rate is too fast to allow fluid transport through the porous matrix, the pore fluid pressure can be defined in terms of the local volumetric strain. In this case, the pore fluid significantly increases the strength and stiffness in hydrostatic compression, since the fluid must be compressed to allow pore collapse.

To illustrate the qualitative effect of the pore fluid, first consider the elastic-plastic response of an idealized incompressible, thick spherical shell. The analytical solution is an effective stress formulation of Carroll and Holt's classic result [8], and is plotted in

Fig. 4. As the shell is compressed plastically, the accumulated fluid pressure shifts the elastic center for the matrix material, which is implemented as an isotropic backstress ($\bar{\zeta}$) in the continuum model. The hydrostatic compressive strength ($\bar{X}$) is defined relative to the shifted elastic center, and also evolves with plastic deformation.

Figure 4 shows the meridional profile of the Arenisca yield surface for an initial and plastically-compressed state. Arenisca uses a poroelastic relation along with an empirical strain-to-yield model (not the spherical shell idealization) to evolve the material properties. This approach allows the model to be parameterized using only data for the drained material and the fluid equation of state, and has desirable traits such as the ability to reduce to the response of the drained material in the limit as the fluid bulk modulus goes to zero.

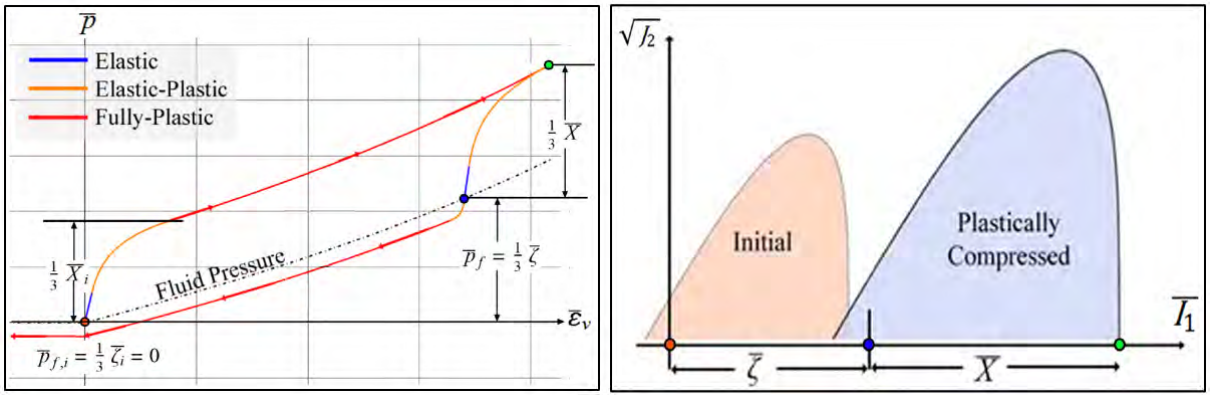

Figure 4: Hydrostatic load-unload response for an incompressible, thick spherical shell with a pore fluid (LEFT) and combined hardening mechanisms for a continuum model of the fluid effects (RIGHT).

The isotropic backstress creates an evolving yield surface vertex, and the hardening laws for the fluid model are highly nonlinear. Both of these model attributes can be problematic for many traditional plasticity solution methods. Arenisca employs a novel solution method, which combines bisection on the consistency parameter with a transformed-space, closest-point return to compute the updated stress and internal state variables. The method is quite robust, and allows for complex model features while avoiding the need to evaluate gradients of the yield function.

2.4 Visualization

The material deformation state can be better visualized by rendering the particles not as points or disks, but as parallelograms, constructed from the original rectangular particle geometry with the deformation gradient tensor. An example of this is shown in Fig. 9, which helps to illustrate the shear bulking that occurs with an associative Drucker-Prager model.

A new approach was taken to visualize the stress state in the target during penetra-

tion, by creating a CMYK color map of a 2D space with the hydrostatic pressure as the abscissa and the magnitude of the shear stress as the ordinate. To distinguish between triaxial extension (TXE) and triaxial compression (TXC), the path of selected particles was rendered along with the initial yield surface in 3D principal stress space. A representative example is given in Fig. 5, which shows that while much of the loading is in triaxial compression, the stress path spans the full range of Lode angles. This suggests that third invariant dependence in the yield strength may improve the predictive capability of the simulations.

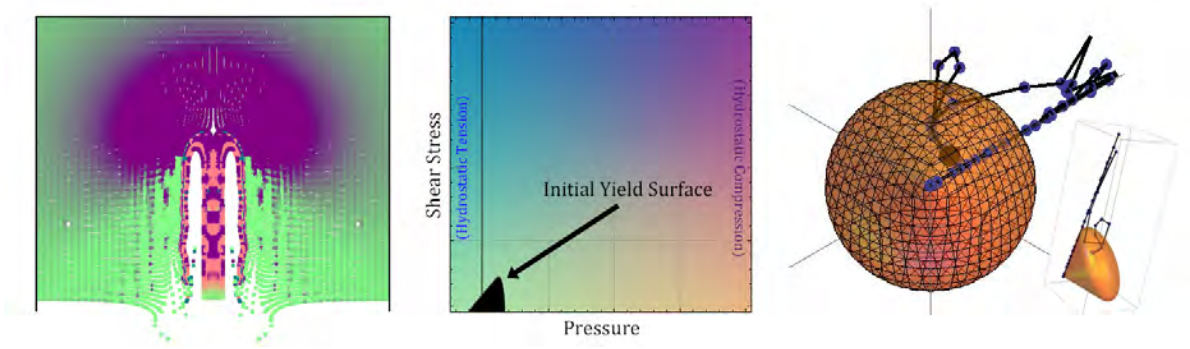

Figure 5: Target stress state during shaped-charge jet penetration (LEFT) visualized through a 2D color map in pressure-shear space (CENTER). The path through principal stress space of a target particle near the penetrator tip is shown (RIGHT) showing an octahedral view with a 3D view inset.

3 RESULTS

The Uintah computational framework has been used along with the Arenisca constitutive model to investigate the effect of a wide range of model features on the penetration simulation results. While the Uintah/Arenisca tools are open source, some quantitative details of the key simulation results in this section are proprietary and therefore omitted. Unless otherwise stated all simulations use GIMP and are axisymmetric, with a discrete jet description and an Arenisca model of a drained sandstone target. In some cases, there is a layer of steel on the surface of the target to represent the wellbore casing.

3.1 MPM Integrator

Figure 6 compares the simulation results for a *plane strain* 2D penetration simulation using the GIMP and CPDI integration methods. The two methods produce clear differences in the penetration channel. Similarities to a solution with a higher-order B-spline method (not shown) suggest that the CPDI integrator might be more accurate, but further validation and convergence studies are needed to support this hypothesis.

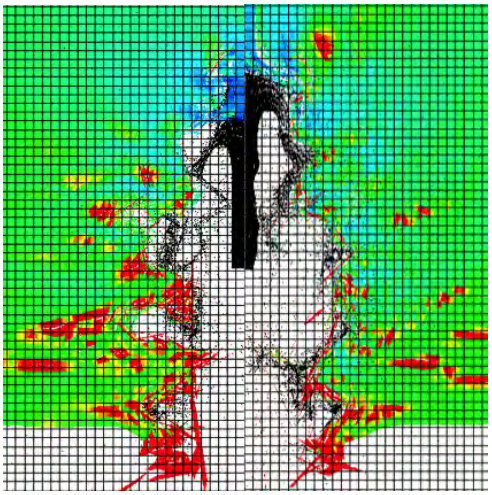

Figure 6: Comparison of a 2D *plain strain* penetration channel for the GIMP (LEFT) and CPDI (RIGHT) integration method.

3.2 Depth of penetration (DOP) vs. pore pressure and confining stress

With pressure-dependent shear strength, the depth of penetration should decrease with confining stress. This behavior is observed in Fig. 7, which shows the penetration channel for a range of confinement levels. For low values of the confining pressure the results of an axisymmetric simulation are unrealistic, since they cannot capture the formation of radial cracks that would occur when shooting a jet into an unconfined target.

To illustrate the effect of the fluid model, Fig. 8 shows the formation of the penetration channel into a drained and undrained target material with zero initial pore pressure and confining stress. The results correctly predict an increased depth of penetration with pore fluid. While the difference is small, it is significant since this is exclusively due to deformation-induced pore pressure. A more pronounced effect can be produced by specifying an initial pore pressure, but this masks the effect of the evolving isotropic backstress.

3.3 Shear bulking control with nonassociativity and porosity

When modeling a nonporous material, the hydrostatic compressive strength is set to a stress beyond that which will occur in the target material, so the cap has no effect on the material strength. This reduces the yield criterion to a simple Drucker-Prager model. If an associative flow law is used, yielding in shear will produce significant plastic dilatation, which causes unrealistic results as shown in Fig. 9. This leads to numerical difficulties as the expanded particles are ejected from the penetration channel at unrealistic velocities.

To mitigate this "shear bulking effect", a nonassociative flow law can be specified to reduce the dilatational component of the plastic flow, but possibly at the cost of losing well-posedness of the solution [12, 10]. Interestingly, a similar effect can be achieved by

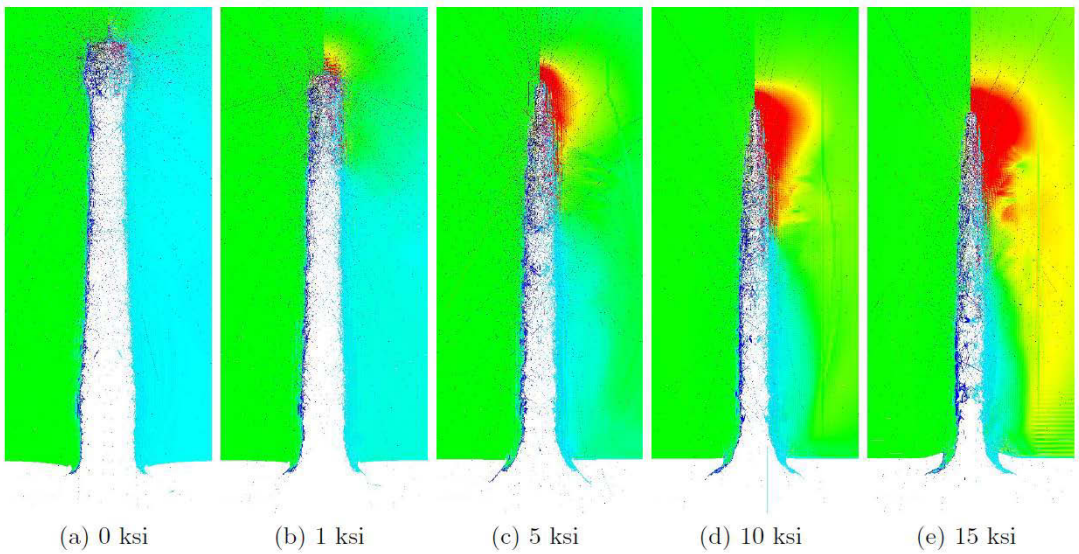

(a) 0 ksi (b) 1 ksi (c) 5 ksi (d) 10 ksi (e) 15 ksi

Figure 7: 2D axisymmetric simulation of penetration into a drained sandstone target for various value of confining stress. Confining pressure increases from left to right, and the depth of penetration decreases with confinement.

parameterizing the crush curve so that dilatation causes the cap to retract, (in effect introducing porosity) so that subsequent compression can collapse the expanded volume. As shown in Fig. 9, the cap retraction approach produces a nearly identical result to that obtained with nonassociativity.

3.4 Variability and Scale effects

Statistical variability and scale effects are necessary to achieve realistic fracture patterns in brittle material failure [6]. Figure 10 shows the distribution of pressure in the penetration channel with scale-dependent variability. For each simulation the average scale-dependent strength is the same, but the Weibull modulus governing the distribution of particle strengths around this average value is varied. For a large degree of variability the presence of extremely weak elements allows a significant increase in the depth of penetration. As the variability is reduced from a nominal value to allow no variability the effect is less dramatic, but yielding of weaker elements is seen to relieve some of the residual stresses in the penetration channel (red zones in Fig. 10).

4 CONCLUSIONS

The computational approach presented herein allows for analysis of shaped-charge penetration into a variety of target material, and is well suited for the development of wellbore perforation technology. The results presented show that the geometry of the penetration channel and the region of damaged material depend on the selection and parameterization of a wide range of model features. Key experimental trends have been reproduced

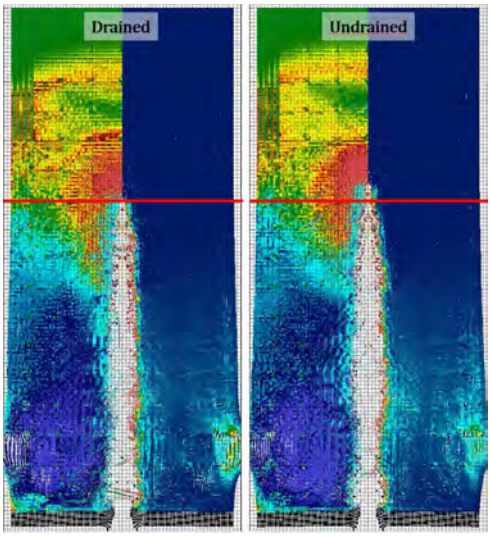

Figure 8: Penetration channel for a drained (LEFT) and undrained (RIGHT) target material with zero initial pore pressure and confining stress showing the correct trend in depth of penetration. For each simulation the left side shows contours of pressure, and the right shows volumetric plastic strain.

with the existing model features; further development will likely produce quantitatively predictive results.

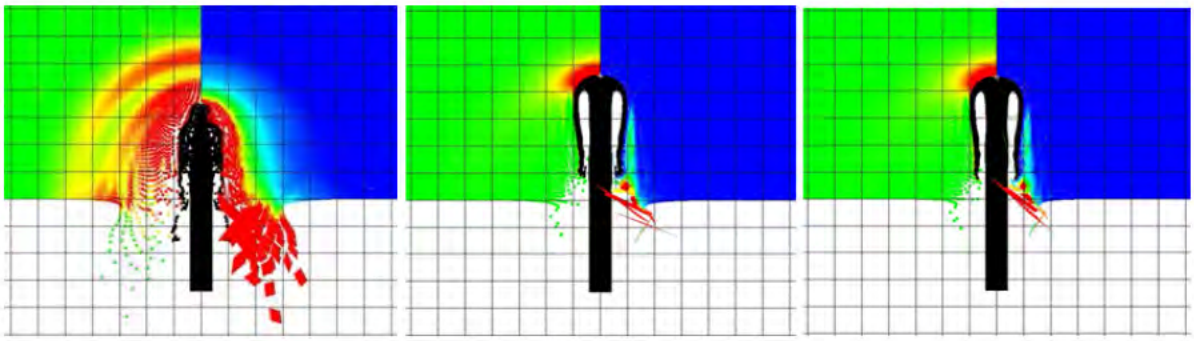

Figure 9: Penetration of an aluminum rod into a Drucker-Prager target showing shear bulking from plastic deformation (LEFT). The dilatation is limited with introduction of porosity (CENTER) and with nonassociativity (RIGHT). In each image the left side shows pressure, and the right shows volumetric plastic strain with deformed glyph visualization to show the deformation state of each particle.

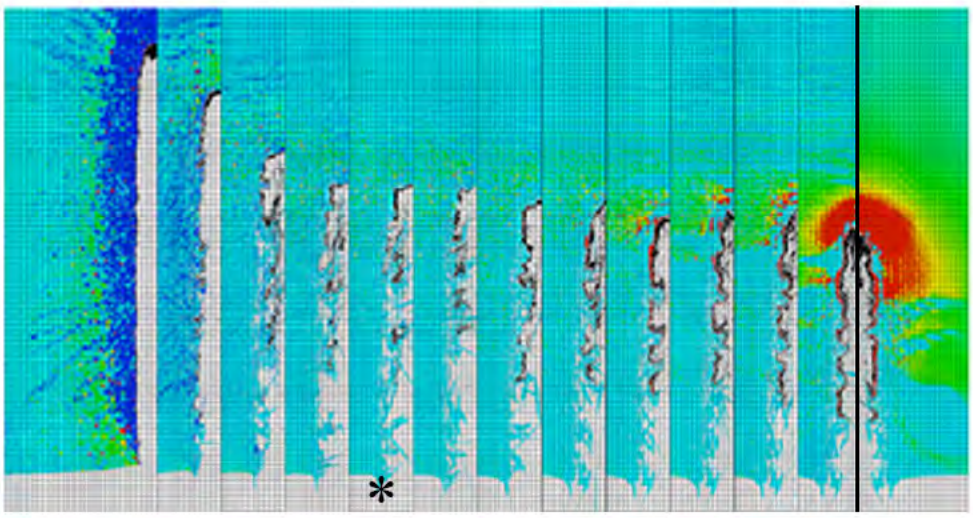

Figure 10: The effect of scale-dependent variability on the penetration channel, with variability decreasing from left to right. Contours show residual pressure in the target material. The reflected image on the far right shows the results with scale effects but no variability. The (*) denotes the simulation with the best available value for the Weibull modulus of the strength distribution.

REFERENCES

[1] Bardenhagen, S. G., and E. M. Kober. The generalized interpolation material point method. *Computer Modeling in Engineering and Sciences* 5.6 (2004): 477-496.

[2] Burghardt, J. B Leavy, J. Guilkey, Z. Xue, R.M. Brannon. Application of Uintah-MPM to shaped charge jet penetration of aluminum. *Sidney, Australia : IOP Conference Series: Materials Science and Engineering.* (2010).

[3] Sadeghirad, A., R.M. Brannon, J. Burghardt. A convected particle domain interpolation technique to extend applicability of the material point method for problems involving massive deformations. *Int. J. for Numerical Methods in Engineering.* (2011): 928-952.

[4] Guilkey, J., T. Harman, *et al.* Uintah User Guide Version 1.1. *SCI Institute, University of Utah*, UUSCI-2009-007 (2009).

[5] Homel, M.A. R.M. Brannon, J.W. Colovos, and J.E. Guilkey. *Arenisca: Theory Guide and User's Manual*, University of Utah, Mechanical Engineering, Computational Solid Mechanics, (2014).

[6] Leavy, R.B., R.M. Brannon, and O.E. Strack. The use of sphere indentation experiments to characterize ceramic damage models. *Int. J. of Appl. Ceram. Tech.* 7.5 (2010): 606-615.

[7] Strack, O.E., R.B. Leavy, and R.M. Brannon Aleatory uncertainty and scale effects in computational damage models for failure and fragmentation, *Int. J. Num. Meth. in Engr.*, Accepted March 25, 2014.

[8] Carroll, M. M., and A. C. Holt. Static and Dynamic PoreCollapse Relations for Ductile Porous Materials. *Journal of Applied Physics* 43.4 (2003): 1626-1636.

[9] Brannon, R.M., A.F. Fossum, and O.E. Strack. Kayenta: theory and users guide. *Sandia Report SAND2009-2282* (2009).

[10] Burghardt, J.A., Nonlocal plasticity, instability, and well-posedness of the elastic-plastic initial-boundary value problem. *Diss. The University of Utah*, (2011).

[11] Biot, M. A. Mechanics of deformation and acoustic propagation in porous media. *Journal of applied physics* 33.4 (2004): 1482-1498.

[12] Sandler, I., and D. Rubin, The consequences of non-associated plasticity in dynamic problems. In: *Constitutive Laws for Engineering Materials*, Elsevier Science Publishing Co. Inc. (1987): 345-353